

Effects of chain length on Rouse modes and non-Gaussianity in linear and ring polymer melts

Shota Goto, Kang Kim,^{a)} and Nobuyuki Matubayasi^{b)}

Division of Chemical Engineering, Department of Materials Engineering Science, Graduate School of Engineering Science, Osaka University, Toyonaka, Osaka 560-8531, Japan

(Dated: 17 September 2021)

The dynamics of ring polymer melts are studied via molecular dynamics simulations of the Kremer–Grest bead-spring model. Rouse mode analysis is performed in comparison with linear polymers by changing the chain length. Rouse-like behavior is observed in ring polymers by quantifying the chain length dependence of the Rouse relaxation time, whereas a crossover from Rouse to reptation behavior is observed in linear polymers. Furthermore, the non-Gaussian parameters of the monomer bead displacement and chain center-of-mass displacement are analyzed. It is found that the non-Gaussianity of ring polymers is remarkably suppressed with slight growth for the center-of-mass dynamics at long chain length, which is in contrast to the growth in linear polymers both for the monomer bead and center-of-mass dynamics.

I. INTRODUCTION

The dynamics of polymer melts are governed by topological constraints, and due to the constraints, the viscosity and relaxation time increase drastically with increasing degree of polymerization. Linear chain ends play a significant role in determining the slip motion of a single polymer chain, which is characterized by the well-established reptation model.¹ Recently, another type of topological constraints in polymer has been proposed, namely, ring polymer melts without chain ends.^{2–6}

Various molecular dynamics (MD) simulations have been performed to elucidate the topological constraint effects in ring polymer melts.^{7–14} In this regard, the chain length N dependence of dynamical properties is the central topic. Tsolou *et al.* reported MD simulation results of a united-atom model for ring polyethylene melts with N ranging from 24 to 400.⁹ They demonstrated that the Rouse model is approximately appropriate for describing the dynamics, in contrast to the cases of linear polymer analogues. Halverson *et al.* used a coarse-grained bead-spring model for ring polymers with N ranging from 100 to 1600.^{10,11} The diffusion coefficient D obeys a scaling $D \sim N^{-2.4}$ for large N —interestingly, this is similar to that observed in linear polymer melts. In contrast, the zero-shear viscosity exhibits a chain length dependence $\eta \sim N^{1.4}$, which is weaker than that predicted by the reptation model.

The dynamics of ring polymer melts have been examined using the dynamic structure factor measured by neutron scattering experiments.^{15–19} Brás *et al.* reported the non-Gaussian parameter (NGP) of pure poly(ethylene oxide) (PEO) rings.¹⁶ The NGP characterizes the degree of the deviation of the distribution function of the monomer displacement from the Gaussian distribution, which is important when discussing the relationship between MD simulations and scattering experiments.²⁰ Notably, the NGP has frequently been analyzed to characterize heterogeneous dynamics, which is attributed to

cage effects in glass-forming liquids.^{21–23} However, the chain length dependence of NGP in ring polymers remains scarcely analyzed. Furthermore, this analysis can be also important when considering the recent microscopic theory predicting $D \sim N^{-2}$ in ring polymer melts, which was formulated in analogy with the cage effects of soft colloid suspensions.²⁴

In this study, we performed MD simulations using the Kremer–Grest bead-spring model with different chain lengths ($N = 5–400$) for both linear and ring polymer melts. First, we analyzed the Rouse modes and determined the chain length dependence of the relaxation time. Then, we calculated the NGP of the monomer bead displacement, and investigated its chain length dependence. The combined results enable us to thoroughly assess the similarities and differences of the chain-end effects on the dynamics between linear and ring polymer melts.

II. MODEL AND SIMULATIONS

We performed MD simulations using the standard Kremer–Grest model for linear and ring polymer melts, where the polymer chain comprises N monomer beads of mass m and diameter σ .²⁵ We utilized three types of inter-particle potentials, as follows. The Lennard-Jones (LJ) potential

$$U_{\text{LJ}}(r) = 4\epsilon_{\text{LJ}} \left[\left(\frac{\sigma}{r} \right)^{12} - \left(\frac{\sigma}{r} \right)^6 \right] + C, \quad (1)$$

acts between all pairs of monomer beads, where r and ϵ_{LJ} denote the distance between two monomers and the energy scale of the LJ potential, respectively. The LJ potential is truncated at the cut-off distance of $r_c = 2.5\sigma$, and the constant C guarantees that the potential energy shifts to zero at $r = r_c$. The bonding potential between two neighboring monomer beads is given by a finitely extensible nonlinear elastic (FENE) potential,

$$U_{\text{FENE}}(r) = -\frac{1}{2}KR_0^2 \ln \left[1 - \left(\frac{r}{R_0} \right)^2 \right] \quad (2)$$

for $r < R_0$, where K and R_0 represent the spring constant and the maximum length of the FENE bond, respectively. We used

^{a)}Electronic mail: kk@cheng.es.osaka-u.ac.jp

^{b)}Electronic mail: nobuyuki@cheng.es.osaka-u.ac.jp

the values of $K = 30\varepsilon_{\text{LJ}}/\sigma^2$ and $R_0 = 1.5\sigma$. Finally, the bending angle θ formed by three consecutive monomer beads along the polymer chain is controlled by

$$U_{\text{bend}}(\theta) = k_\theta [1 - \cos(\theta - \theta_0)], \quad (3)$$

where k_θ denotes the associated bending energy. We set the bending energy and equilibrium angle as $k_\theta = 1.5\varepsilon_{\text{LJ}}$ and $\theta_0 = 180^\circ$, respectively.

Henceforth, the length, energy, and time are measured in units of σ , ε_{LJ} , and $\sigma(m/\varepsilon_{\text{LJ}})^{1/2}$, respectively. The temperature is presented in units of $\varepsilon_{\text{LJ}}/k_B$, where k_B is the Boltzmann constant. The system contains M polymer chains in a three-dimensional cubic box of volume V under periodic boundary conditions. We studied several combinations of the chain length N and the number of chains M for both linear and ring polymer systems, $(N, M) = (5, 2000), (10, 1000), (20, 500), (40, 250), (100, 200), (200, 100)$, and $(400, 50)$. The number density of the monomer beads $\rho = (N \times M)/V$ and the temperature T were fixed as $\rho = 0.85$ and $T = 1.0$, respectively, throughout the simulations. We performed the MD simulations using the Large-scale Atomic/Molecular Massively Parallel Simulator (LAMMPS).²⁶ The NVT ensemble with the Nosé–Hoover thermostat was used with a time step Δt of 0.01. We analyzed the chain length dependence of the radius of gyration and the center-of-mass diffusion coefficient and confirmed that our results reproduce the results reported in previous studies (results not shown).^{10,11} In addition, we confirmed the entanglement length $N_e \approx 28$ in linear polymer melts with $N = 400$ by using the primitive path analysis.²⁷ The used code is available from <https://github.com/t-murash/USER-PPA> (see also Ref. 28).

The Rouse model is the standard model for the polymer chain dynamics, where the normal coordinates $\mathbf{X}_p(t)$, so-called Rouse modes, are constructed from the position of the n -th monomer bead $\mathbf{r}_n(t)$ at a time t for $n = 1, 2, 3, \dots, N$. Here, we provide several expressions in the Rouse model, which we employ to analyze our MD results. The Rouse mode analysis for the linear chain is described in Ref. 29. Furthermore, the formula for the ring polymer chain was described in previous papers.^{9,30,31} To make this paper self-contained, we summarize the formulation of the Rouse model for the ring polymer chain in Appendix. The expressions of the normal coordinates $\mathbf{X}_{p,\text{linear}}(t)$ and $\mathbf{X}_{p,\text{ring}}(t)$ for linear and ring polymer chains can respectively be expressed as

$$\mathbf{X}_{p,\text{linear}}(t) = \sqrt{\frac{2 - \delta_{p,0}}{N}} \sum_{n=1}^N \mathbf{r}_n(t) \cos\left(\frac{\pi p(n - 1/2)}{N}\right), \quad (4)$$

$$\mathbf{X}_{p,\text{ring}}(t) = \sqrt{\frac{1}{N}} \sum_{n=1}^N \mathbf{r}_n(t) \left[\cos\left(\frac{2\pi pn}{N}\right) + \sin\left(\frac{2\pi pn}{N}\right) \right], \quad (5)$$

where $p (= 0, 1, \dots, N - 1)$ is the mode index, and δ denotes the Kronecker delta. The $p = 0$ mode describes the center-of-mass translation of the chain, whereas the $p > 0$ modes characterize the internal dynamics of the subchains composed of N/p beads.

The static correlation of the Rouse mode $\langle \mathbf{X}_p(0)^2 \rangle$ can be related to the mean square distance of two beads b^2 through

$$\langle \mathbf{X}_{p,\text{linear}}(0)^2 \rangle = \frac{b^2}{4 \sin^2\left(\frac{\pi p}{2N}\right)}, \quad (6)$$

$$\langle \mathbf{X}_{p,\text{ring}}(0)^2 \rangle = \frac{b^2}{4 \sin^2\left(\frac{\pi p}{N}\right)}, \quad (7)$$

for linear and ring polymers, respectively. Here, $\langle \dots \rangle$ denotes an ensemble average.

Each normal coordinate exhibits the Brownian motion in the Rouse model, causing the exponential decay of the auto-correlation function, $\langle \mathbf{X}_p(t) \cdot \mathbf{X}_p(0) \rangle$. The Rouse relaxation times $\tau_{p,\text{linear}}$ and $\tau_{p,\text{ring}}$ for linear and ring polymer chains are respectively given by

$$\tau_{p,\text{linear}} = \frac{\zeta}{4k \sin^2\left(\frac{\pi p}{2N}\right)}, \quad (8)$$

$$\tau_{p,\text{ring}} = \frac{\zeta}{4k \sin^2\left(\frac{\pi p}{N}\right)}, \quad (9)$$

where ζ is the effective hydrodynamic friction coefficient and k represents the harmonic spring constant between two neighboring monomer beads. As noted in Appendix k is equal to $3k_B T/b^2$. The differences of $\langle \mathbf{X}_p(0)^2 \rangle$ and τ_p between linear and ring polymers appear in the phases of the sine functions. The Rouse modes of p and $N - p$ are degenerate in the case of the ring polymer (see Appendix). Correspondingly, $\langle \mathbf{X}_p(0)^2 \rangle$ and τ_p as functions of p are symmetric with respect to the reflection at $p = N/2$. On the other hand, for linear chains, $\langle \mathbf{X}_p(0)^2 \rangle$ and τ_p decrease monotonically with p in the Rouse model. In the continuum limit of $p/N \ll 1$, both $\tau_{p,\text{linear}}$ and $\tau_{p,\text{ring}}$ exhibit a scaling behavior $(N/p)^2$ within the Rouse model.

The motions of monomer beads are described typically by the mean square displacement (MSD) averaged over all the monomers of a chain, which is defined as

$$g_1(t) = \langle r^2(t) \rangle = \left\langle \frac{1}{N} \sum_{n=1}^N |\mathbf{r}_n(t) - \mathbf{r}_n(0)|^2 \right\rangle. \quad (10)$$

The NGP of the monomer bead displacement is defined by

$$\alpha_2^{\text{mon}}(t) = \frac{3\langle r^4(t) \rangle}{5\langle r^2(t) \rangle^2} - 1, \quad (11)$$

which measures non-Gaussianity, *i.e.*, the degree of the deviation of the distribution function of the monomer bead displacement from the Gaussian form during the time interval t . In addition, the MSD of the center-of-mass of chains is examined from

$$g_3(t) = \langle R^2(t) \rangle = \left\langle \frac{1}{M} \sum_{m=1}^M |\mathbf{R}_m(t) - \mathbf{R}_m(0)|^2 \right\rangle, \quad (12)$$

where $\mathbf{R}_m(t)$ is the position of the center-of-mass of the chain m at time t . The corresponding NGP of the center-of-mass

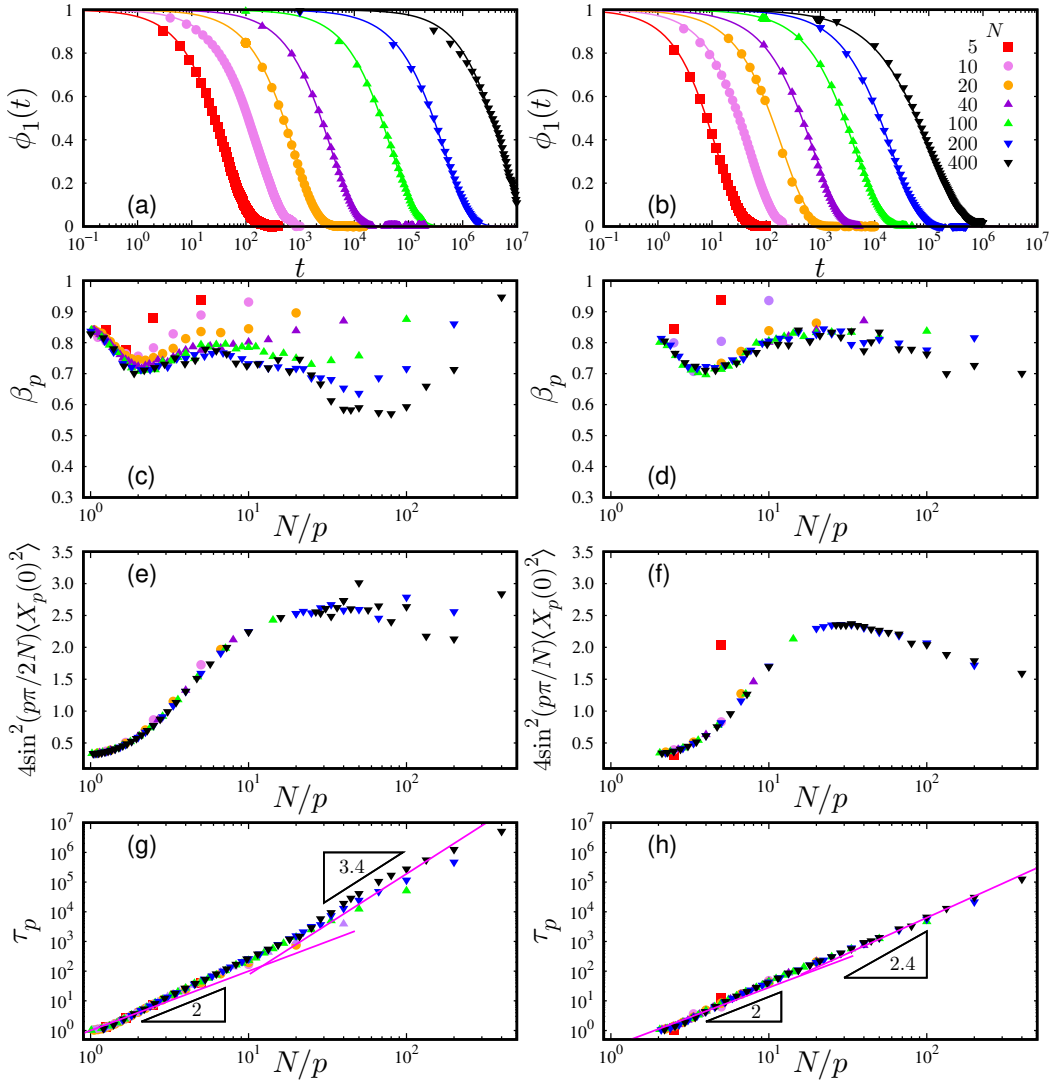


FIG. 1. Normalized autocorrelation function $\phi_1(t)$ of the Rouse mode $p = 1$ for linear (a) and ring (b) polymers. Symbols and lines represent MD simulation results and the fitting curves using the Kohlrausch–Williams–Watts function, $\exp[-(t/\tau_p)^{\beta_p}]$. The exponent β_p is plotted as a function of N/p for linear (c) and ring (d) polymers. Normalized amplitude of autocorrelations of the Rouse mode, $4 \sin^2(\pi p/(2N)) \langle X_p(0)^2 \rangle$ (e) and $4 \sin^2(\pi p/N) \langle X_p(0)^2 \rangle$ (f), are plotted as a function of N/p for linear and ring polymers, respectively. Rouse relaxation time τ_p as a function of N/p for linear (g) and ring (h) polymers. Two scaling behaviors, i.e., the Rouse model behavior $\tau_p \sim (N/p)^2$ and the reptation model behavior $\tau_p \sim (N/p)^{3.4}$, are represented in (g). In (h), $\tau_p \sim (N/p)^2$ is indicated for smaller N/p , whereas the different power-law $\tau_p \sim (N/p)^{2.4}$ is observed for larger N/p . In (d), (f), and (h), the results for $N/p < 2$ are omitted because of the symmetric structure of N/p dependencies on $\langle X_p(0)^2 \rangle$ and τ_p (see Eqs. (5), (7) and (9)). Note that only two points with $p = 1$ and 2 are plotted for $N = 5$ ring polymers, where each ring tends to form a pentagonal structure, causing fluctuations more than other length chains.

displacement is defined by

$$a_2^{\text{com}}(t) = \frac{3 \langle R^4(t) \rangle}{5 \langle R^2(t) \rangle^2} - 1. \quad (13)$$

The NGP of monomer beads was analyzed via MD simulations of linear polymer melts with the chain length of $N = 5 - 160$.³² Furthermore, the NGP of supercooled polymer melts was reported with $N = 10^{33}$ and $N = 64$.^{34,35}

III. RESULTS AND DISCUSSION

The normalized autocorrelation function of the p -th Rouse mode is given by

$$\phi_p(t) = \frac{\langle \mathbf{X}_p(t) \cdot \mathbf{X}_p(0) \rangle}{\langle \mathbf{X}_p(0)^2 \rangle}. \quad (14)$$

The results of the slowest mode $\phi_1(t)$ are plotted in Fig. 1 by changing the chain length N for linear (a) and ring (b) polymer melts. For each Rouse mode p , $\phi_p(t)$ is fitted using the Kohlrausch–Williams–Watts (KWW) function,

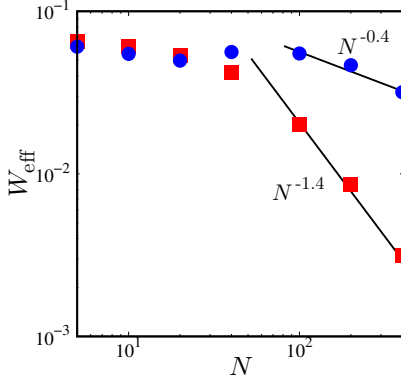


FIG. 2. Chain length N dependence of the effective segmental relaxation rate W_{eff} for linear (squares) and ring (circles) polymers. Two straight lines are eye guides indicating, $W_{\text{eff}} \sim N^{-1.4}$ and $W_{\text{eff}} \sim N^{-0.4}$.

$\exp[-(t/\tau_p^*)^{\beta_p}]$, with the KWW relaxation time τ_p^* . $\beta_p (< 1)$ represents the degree of non-exponentiality of $\phi_p(t)$.³⁶ In Fig. 1(c) and (d), β_p is plotted as a function of N/p for linear and ring polymers, respectively. As demonstrated in Ref. 37, β_p deviates from unity and shows a minimum at the slowing down length $N_s \approx 2$. Another minimum of approximate 0.6 is found at around the entanglement length scale $N_e \approx 28$.^{38,39} As seen in Fig. 1(d), β_p of ring polymers shows a minimum at $N_s \approx 4$, which is the same length scale of $N_s \approx 2$ considering the difference in the phase of the Rouse mode between linear and ring polymers. Furthermore, the non-exponentiality is also found at $N \gtrsim 10^2$ and is weaker for the ring polymers with $\beta_p \approx 0.8$ than for the linear polymers.

In Fig. 1(e) and (f), the normalized amplitudes $4 \sin^2(\pi p/(2N)) \langle \mathbf{X}_p(0)^2 \rangle$ and $4 \sin^2(\pi p/N) \langle \mathbf{X}_p(0)^2 \rangle$ are plotted as a function of N/p for linear and ring polymers, respectively. As the chain length scale N/p increases, $4 \sin^2(\pi p/(2N)) \langle \mathbf{X}_p(0)^2 \rangle$ of linear polymers levels off beyond the entanglement length scale $N_e \approx 28$,^{38,39} whereas $4 \sin^2(\pi p/N) \langle \mathbf{X}_p(0)^2 \rangle$ of ring polymers gradually decreases with increasing N/p . This behavior is actually consistent with the observation that the structure of the ring polymer chain becomes more compact than that of the linear polymer. In fact, N dependence of the mean square radius of gyration R_g^2 approaches a scaling of $N^{2/3}$ in ring polymers, which is distinct from the Gaussian behavior $R_g^2 \sim N$ observed in linear polymers.¹⁰

The effective Rouse relaxation time of the p -th mode is calculated by

$$\tau_p = \int_0^\infty \exp[-(t/\tau_p^*)^{\beta_p}] dt = \frac{\tau_p^*}{\beta_p} \Gamma\left(\frac{1}{\beta_p}\right), \quad (15)$$

where $\Gamma(x)$ is the Gamma function. The Rouse relaxation time τ_p is plotted as a function of N/p in Fig. 1 for linear (g) and

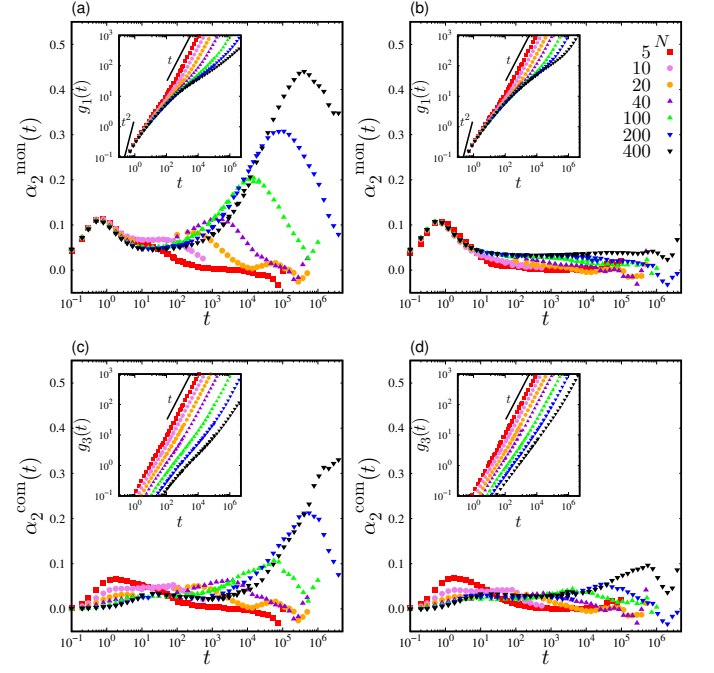


FIG. 3. Non-Gaussian parameters of monomer beads $\alpha_2^{\text{mon}}(t)$ and center-of-mass $\alpha_2^{\text{com}}(t)$ for linear [(a) and (c)] and ring [(b) and (d)] polymers. Inset: Mean square displacements of monomer beads $\langle r^2(t) \rangle$ and the center-of-mass $\langle R^2(t) \rangle$. The solid lines represent ballistic motion ($\sim t^2$) and diffusive behavior ($\sim t$).

ring (h) polymer melts. In linear polymer melts, τ_p rapidly deviates from the Rouse regime $(N/p)^2$ as the chain length N is increases. In particular, the power-law behavior $\tau_p \sim (N/p)^{3.4}$ was observed, indicating entanglement effects.^{38,39} This crossover from the Rouse to the reptation behavior was reported in Refs. 38 and 39. τ_p of ring polymers also deviates from the Rouse-like power-law behavior with increasing N/p . However, the exponent becomes 2.4, which is smaller than that of linear polymers for the chain lengths investigated in this study.

Further, it is important to compare the segmental relaxation rate $W_{\text{eff}} = 3k_B T / \zeta b^2 = k / \zeta$ between linear and ring polymer melts, which is related to the Rouse relaxation time τ_p (see Eqs. (8) and (9)). Specifically, we evaluated W_{eff} using the slowest mode ($p = 1$) by

$$W_{\text{eff,linear}} = 1/[4\tau_{1,\text{linear}} \sin^2(\pi/2N)], \quad (16)$$

$$W_{\text{eff,ring}} = 1/[4\tau_{1,\text{ring}} \sin^2(\pi/N)], \quad (17)$$

for linear and ring polymers, respectively, and the results are plotted in Fig. 2. For linear polymers, W_{eff} exhibits a roughly constant independent of N up to the entanglement length $N_e \approx 28$. A similar value is also observed for ring polymers, indicating the same Rouse dynamics in melts of linear and ring chains. The power-law behavior $W_{\text{eff}} \sim N^{-1.4}$ is observed for the longer linear polymer, which is consistent with the scaling of $\tau_p \sim (N/p)^{3.4}$, as demonstrated in Fig. 1(e). Note that N and p are both varied in Fig. 1(e), and the scaling at $p = 1$ is rephrased as $\tau_1 \sim N^{3.4}$ at large N . In contrast, W_{eff}

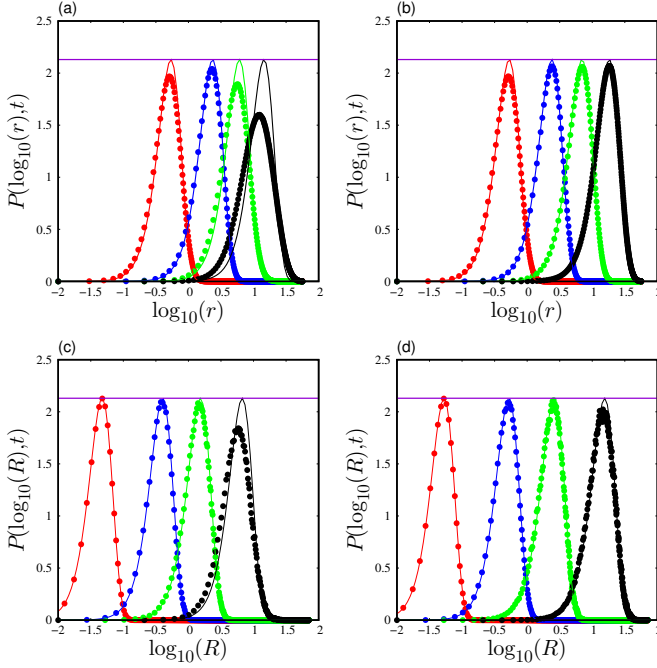


FIG. 4. Probability distributions of the logarithm displacement of monomer beads and center-of-mass, $P(\log_{10}(r), t)$ and $P(\log_{10}(R), t)$, for linear [(a) and (c)] and ring [(b) and (d)] polymers with the chain length $N = 400$. The time t is chosen as $t = 1, 10^2, 10^4$, and 10^6 from left to right. The horizontal line denotes the Gaussian level, $\ln(10)\sqrt{54/\pi}e^{-3/2} \approx 2.13$. The solid curve represent the form using the Gaussian distribution, $G_s(r, t) = [3/(2\pi\langle r^2(t) \rangle)]^{3/2} \exp[-3r^2/(2\langle r^2(t) \rangle)]$ [(a) and (b)] and $G_s(R, t) = [3/(2\pi\langle R^2(t) \rangle)]^{3/2} \exp[-3R^2/(2\langle R^2(t) \rangle)]$ [(c) and (d)] at each time.

of ring polymers shows a weak N dependence and the scaling $W_{\text{eff}} \sim N^{-0.4}$ is observed for the longer chain length $N \gtrsim 100$. This exponent corresponds to the scaling of $\tau_p \sim (N/p)^{2.4}$, as observed in Fig. 1(f).

The NGPs of the segment displacement $\alpha_2^{\text{mon}}(t)$ and the center-of-mass displacement $\alpha_2^{\text{com}}(t)$ were investigated using Eqs. (11) and (13), respectively. Figure 3 shows $\alpha_2^{\text{mon}}(t)$ for linear (a) and ring (b) polymers. For comparison, the time evolutions of MSD $\langle r^2(t) \rangle$ are displayed in inset of Fig. 3(a) and (b). It is seen that $\alpha_2^{\text{mon}}(t)$ exhibits peaks of 0.1 for both linear and ring polymers. The peak occurs at $t \approx 1$, beyond which each segment begins to escape from the regime of ballistic motion, $\langle r^2(t) \rangle \sim t^2$, at small times. The height and position $\alpha_2^{\text{mon}}(t)$ in the ballistic regime are independent of the chain length N , indicating that the effects of polymer chain ends are negligible in this regime, where the effect of the chain connectivity plays the role on the segmental dynamics.³³ For linear polymers, the second peak appears at a larger time regime, where $\langle r^2(t) \rangle$ approaches the diffusive behavior, as demonstrated in Fig. 3(c). The second peak develops for longer time scales with increasing chain length N , which was demonstrated in the previous study.³² The height of the second peak becomes 0.5 for $N = 400$. This non-Gaussianity can be regarded as the chain end effect with higher mobility due to less topological constraints.⁴⁰ Note that the mechanism

of non-Gaussianity in linear polymer melts is different from that of the cage effects in glass-forming liquids.^{21–23} On the contrary, it is unlikely that $\alpha_2^{\text{mon}}(t)$ of ring polymers shows clear peaks for chain lengths up to $N = 400$ despite the diffusive behavior being realized in $\langle r^2(t) \rangle$ at larger time scales (see Fig. 3(d)). This implies that all the monomer beads show similar dynamics in ring polymers without chain ends. The non-Gaussianity of the center-of-mass displacement is additionally examined in Fig. 3 for linear (c) and ring (d) polymers. The behavior of $\alpha_2^{\text{com}}(t)$ is analogous to that of $\alpha_2^{\text{mon}}(t)$ both for linear and ring polymers. However, the first peak of $\alpha_2^{\text{com}}(t)$ at $t \approx 1$ becomes smaller with increasing N for both linear and ring polymers. This indicates that regardless of the chain connectivity, the center-of-mass dynamics is more Gaussian for longer chains. Furthermore, $\alpha_2^{\text{com}}(t)$ of ring polymers with $N = 400$ shows a peak of 0.1 at $t \approx 10^6$, which shows very small non-Gaussianity as the chain length is increased.

Finally, to characterize the difference in the NGP between linear and ring polymers in more detail, we calculated the self-part of the van Hove correlation function $G_s(r, t) = \langle \sum_{n=1}^N \delta(|\mathbf{r}_n(t) - \mathbf{r}_n(0)| - r) \rangle$, i.e., the distribution function of the segmental displacement r at time t . The probability distribution of the logarithm displacement is then defined as $P(\log_{10}(r), t) = \ln(10)4\pi r^3 G_s(r, t)$.^{41–43} It is defined such that the integral $\int_{x_0}^{x_1} P(x, t) dx$ is the fraction of particles whose value of $\log_{10}(r)$ is between x_0 and x_1 . When the Gaussian distribution is assumed as $G_s(r, t) = [3/(2\pi\langle r^2(t) \rangle)]^{3/2} \exp[-3r^2/(2\langle r^2(t) \rangle)]$ with the mean square displacement $\langle r^2(t) \rangle$ at time t , $P(\log_{10}(r), t)$ has a peak of $\ln(10)\sqrt{54/\pi}e^{-3/2} \approx 2.13$ irrespective of time t . In Fig. 4, $P(\log_{10}(r), t)$ is plotted for linear (a) and ring (b) polymers with the chain length $N = 400$ by changing t from 1 to 10^6 . For a comparison, we also showed $P(\log_{10}(R), t)$ determined from the Gaussian distribution $G_s(R, t) = [3/(2\pi\langle R^2(t) \rangle)]^{3/2} \exp[-3R^2/(2\langle R^2(t) \rangle)]$ at each time. As observed in Fig. 4(a), the peak height of $P(\log_{10}(r), t)$ for the linear polymer decreases as t increases. This decrease in the peak indicates that the distribution deviates from the Gaussian behavior and becomes broader, which is also observed in glass-forming liquids.⁴³ Figure 4(b) demonstrates that the peak height of $P(\log_{10}(r), t)$ for ring polymers remains at the Gaussian level, providing clear evidence that the segment displacement follows the Gaussian distribution even for longer time scales.

Furthermore, Fig. 4(c) and Fig. 4(d) show the probability distributions of the center-of-mass displacement $P(\log_{10}(R), t)$ for linear and ring polymers, respectively. The deviation from the Gaussian form $G_s(R, t) = [3/(2\pi\langle R^2(t) \rangle)]^{3/2} \exp[-3R^2/(2\langle R^2(t) \rangle)]$ is noticeable for linear polymers, particularly for longer times. Analogous to Fig. 4(b), $P(\log_{10}(R), t)$ of ring polymers is in accordance with the Gaussian distribution at any time. Note that small deviation from the Gaussian distribution at long times were observed in Fig. 3(d) for the chain length $N = 400$, while the peak value remains the Gaussian level of 2.13. This observation concerning the loss of Gaussianity suggests the possibility that the center-of-mass dynamics of a long ring polymer chain in melts can be influenced by the neighboring rings.

IV. CONCLUSIONS AND FINAL REMARKS

We presented the MD simulation results using the Kremer–Grest model for linear and ring polymer melts with chain lengths up to $N = 400$. We focused on the chain length dependence of the Rouse relaxation time and non-Gaussianity for characterizing both the segmental and center-of-mass mobility with or without chain ends.

For linear polymers, the deviation from the Rouse model behavior becomes remarkable with increasing the chain length N by showing the scaling $\tau_p \sim (N/p)^{3.4}$, which is consistent with previously reported results.¹¹ The NGP of the monomer bead dynamics shows two peaks: the first peak appears on the time scale where the MSD escapes from the segmental ballistic motion, whereas the second peak corresponds to the realization of the diffusive behavior of the MSD. This indicates that the segment dynamics becomes spatially heterogeneous because of the higher mobility of chain ends in the linear polymer chain. The NGP of the center-of-mass dynamics also exhibits two peaks, but the first peak becomes weaker due to less chain connectivity effects as the chain length is increased.

For ring polymers, the Rouse-like behavior with the scaling $\tau_p \sim (N/p)^{2.4}$ was observed. Although the peak of NGP was observed at short times similar to that of linear polymers, the non-Gaussianity was found to be strongly suppressed even for a longer time regime. The segmental dynamics in ring polymers without chain ends becomes spatially homogeneous and the mechanism of the chain motion is essentially different from the reptation model for linear polymers. The center-of-mass dynamics in ring polymers also shows the Gaussian behavior, while a very small non-Gaussianity is observed with increasing chain length suggesting cooperative motions between neighboring rings.

As mentioned in Introduction, Brás *et al.* reported the NGP of the center-of-mass dynamics in PEO ring polymers from a neutron scattering experiment.¹⁶ The molecular weight 5 kg/mol was chosen to be 2.5 times larger than the entanglement mass, which approximately corresponds to the chain length $N = 100$ in the present MD simulation study. The NGP from the neutron scattering experiment shows a peak of 0.2–0.3 at around 30 ns, which corresponds to the crossover from a sub-diffusion to diffusion regime. It seems that the experimental result is not in agreement with the present MD simulation result of $\alpha_2^{\text{com}} \approx 0.1$ with $N = 400$. The effects of the chain lengths and the chemical species of the segments need to be studied in further depths to resolve the difference.

A plausible key feature for topological constraints in ring polymers is an inter-ring threading event.^{44–52} In particular, Michieletto *et al.* have proposed the “random pinning” procedure, wherein some fractions of rings are frozen, to investigate the role of threadings on the dynamics.⁴⁹ They demonstrated that random pinning can enhance the glass-like heterogeneous dynamics in ring polymers. Furthermore, it was reported that the distribution of the center-of-mass displacement deviates from the Gaussian distribution even in a zero “random pinning” field. In contrast, the non-Gaussianity is much weaker in this work, where $\alpha_2^{\text{com}}(t)$ becomes 0.1 with the chain length $N = 400$ without the pinning procedure. One possible in-

terpretation could be that the thermodynamic states analyzed here are different: monomer density $\rho = 0.85$ in this study is frequently used for MD simulations of polymer melts^{10,11}, whereas densities in Ref. 49 were chosen up to $\rho = 0.4$. Therefore, further investigation is necessary for a strict assessment with regard to the monomer density dependence of the non-Gaussianity with increasing the chain length N , which is a subject of future study.

Appendix: Formulation of the Rouse model for ring polymer chain

In the Rouse model, the equation of motion for the polymer chain composed of N beads is given by the following Langevin equation:

$$\zeta \frac{d\mathbf{r}_n}{dt} = -k(2\mathbf{r}_n - \mathbf{r}_{n-1} - \mathbf{r}_{n+1}) + \mathbf{w}_n(t), \quad (\text{A.1})$$

where \mathbf{r}_n represents the coordinates of the n -th bead for $n = 1, 2, 3, \dots, N$ and ζ denotes the effective hydrodynamic friction coefficient. Furthermore, two successive beads are connected by a harmonic spring with the modulus k . Here, the random force \mathbf{w}_n acting on the bead is related to the temperature T and friction coefficient ζ by obeying the fluctuation-dissipation theorem:

$$\langle \mathbf{w}_n(t) \cdot \mathbf{w}_m(t') \rangle = 6k_B T \zeta \delta_{nm} \delta(t - t'). \quad (\text{A.2})$$

According to the statistical description for the freely-jointed chain model, the spring constant k is equal to $3k_B T/b^2$ with the mean square distance b^2 between two beads. Note that the periodic boundary conditions

$$\mathbf{r}_0 = \mathbf{r}_N, \quad \mathbf{r}_{N+1} = \mathbf{r}_1 \quad (\text{A.3})$$

should be imposed on the ring polymer chain. If we define two $N \times 3$ matrices, $\mathbf{R} = (\mathbf{r}_1, \mathbf{r}_2, \mathbf{r}_3, \dots, \mathbf{r}_N)^T$ and $\mathbf{W} = \zeta^{-1}(\mathbf{w}_1, \mathbf{w}_2, \mathbf{w}_3, \dots, \mathbf{w}_N)^T$ (the superscript T denotes the transpose), Eq.(A.1) can be expressed as

$$\frac{d\mathbf{R}}{dt} = -\frac{k}{\zeta} \mathbf{A} \mathbf{R} + \mathbf{W}, \quad (\text{A.4})$$

with the $N \times N$ matrix \mathbf{A} :

$$\mathbf{A} = \begin{pmatrix} 2 & -1 & 0 & \cdots & 0 & 0 & -1 \\ -1 & 2 & -1 & \cdots & 0 & 0 & 0 \\ 0 & -1 & 2 & \cdots & 0 & 0 & 0 \\ 0 & 0 & -1 & \cdots & 0 & 0 & 0 \\ \vdots & & & \ddots & & & \vdots \\ 0 & 0 & 0 & \cdots & -1 & 2 & -1 \\ -1 & 0 & 0 & \cdots & 0 & -1 & 2 \end{pmatrix}. \quad (\text{A.5})$$

Equation (A.4) can be solved by the diagonalization of the matrix \mathbf{A} . The eigenvalue λ equation is given as

$$(\mathbf{A} - \lambda \mathbf{E}) \mathbf{F} = 0, \quad (\text{A.6})$$

with the eigenvector $\mathbf{F} = (f_1, f_2, f_3, \dots, f_N)^T$ and the unit matrix \mathbf{E} . If the function form of f_n is assumed to be

$$f_n = z^n, \quad (\text{A.7})$$

with the complex number z , Eq. (A.6) reduces to the following multiple linear equations:

$$(2 - \lambda)z - z^2 - z^N = 0, \quad (\text{A.8})$$

$$\vdots$$

$$-z^{n-1} + (2 - \lambda)z^n - z^{n+1} = 0, \quad (\text{A.9})$$

$$\vdots$$

$$-z - z^{N-1} + (2 - \lambda)z^N = 0. \quad (\text{A.10})$$

From Eq. (A.9), the characteristic equation

$$-1 + (2 - \lambda)z - z^2 = 0, \quad (\text{A.11})$$

is obtained. The two roots are denoted as z_1 and z_2 , then

$$z_1 + z_2 = 2 - \lambda, \quad z_1 z_2 = 1. \quad (\text{A.12})$$

Furthermore, the function form of z is assumed to be

$$z_1 = e^{i\theta}, \quad z_2 = e^{-i\theta} \quad (\text{A.13})$$

such that $z_1 z_2 = 1$ with the imaginary unit i and an arbitrary argument θ in the complex plane. We obtain the identity:

$$e^{iN\theta} = 1 \quad (\text{A.14})$$

to satisfy Eqs. (A.8), (A.9), and (A.10) in a consistent manner. The argument θ should be

$$\theta = \frac{2\pi p}{N}, \quad (\text{A.15})$$

where p denotes the Rouse mode index with $p = 0, 1, 2, \dots, N - 1$. Thus, the eigenvalue of the mode p is obtained as

$$\lambda_p = 2 - (z_1 + z_2) = 2 \left(1 - \cos \left(\frac{2\pi p}{N} \right) \right) = 4 \sin^2 \left(\frac{\pi p}{N} \right). \quad (\text{A.16})$$

Note that $\lambda_p = \lambda_{N-p}$. Accordingly, the Rouse modes are symmetric with respect to the reflection at $p = N/2$ and the two modes of $p = n$ and $p = N - n$ are degenerate for ring polymers.

The general solution for the element of the eigenvector \mathbf{F} can be given by

$$f_{n,p} = A e^{in\theta} + A^* e^{-in\theta}, \quad (\text{A.17})$$

with a complex constant A . Note that Eq. (A.17) ensures $f_{n,p} = f_{n,p}^*$, where the superscript $*$ denotes the complex conjugate. The orthogonal condition for $f_{n,p}$ is given by

$$\sum_{n=1}^N f_{n,p} f_{n,q}^* = \delta_{p,q}. \quad (\text{A.18})$$

The l.h.s of Eq. (A.18) can be expressed as

$$\begin{aligned} & \sum_{n=1}^N (A e^{i2\pi np/N} + A^* e^{-i2\pi np/N}) \times (A^* e^{-i2\pi nq/N} + A e^{i2\pi nq/N}) \\ &= \sum_{n=1}^N (A^2 e^{i2\pi n(p+q)/N} + A A^* e^{i2\pi n(p-q)/N} \\ & \quad + A^* A e^{-i2\pi n(p-q)/N} + (A^*)^2 e^{-i2\pi n(p+q)/N}). \end{aligned} \quad (\text{A.19})$$

To obtain the condition for determining A , we assume the special case $p + q = N$ ($p \neq q$); then, Eq. (A.19) further reduces to

$$\sum_{i=1}^N (A^2 + (A^*)^2), \quad (\text{A.20})$$

where $\sum_{n=1}^N e^{i2\pi n(p-q)/N} = 0$ is used. Thus, the first relationship $A^2 + (A^*)^2 = 0$ is obtained from the orthogonal condition, Eq. (A.18). Furthermore, the normalization condition for $f_{n,p}$ is given by

$$\sum_{n=1}^N f_{n,p} f_{n,p}^* = 1, \quad (\text{A.21})$$

which can be expressed at $p \neq 0$ or $N/2$ as

$$\sum_{n=1}^N (A^2 e^{i4\pi np/N} + 2A A^* + (A^*)^2 e^{-i4\pi np/N}) = \sum_{i=1}^N 2A A^* = 1, \quad (\text{A.22})$$

and the second relationship $A A^* = 1/(2N)$ is obtained. We again use $\sum_{i=1}^N e^{i4\pi np/N} = 0$ in the cases of $p \neq 0$ and $p \neq N/2$. Note that $A A^* = 1/(2N)$ is also obtained in the two cases $p = 0$ and $p = N/2$ according to $A^2 + (A^*)^2 = 0$. From the two relationships, the complex constant A can be determined, and its expression is chosen from four candidates: $A = (1 + i)/(2\sqrt{N})$, $(-1 - i)/(2\sqrt{N})$, $(-1 + i)/(2\sqrt{N})$, and $(1 - i)/(2\sqrt{N})$. The functional form of $f_{n,p}$ is then determined as

$$f_{n,p} = \sqrt{\frac{1}{N}} \left[\cos \left(\frac{2\pi np}{N} \right) + \sin \left(\frac{2\pi np}{N} \right) \right], \quad (\text{A.23})$$

and Eq. (A.23) satisfies Eq. (A.18). Note that a different expression for $f_{n,p}$ is described and utilized in the path integral molecular dynamics.⁵³

Here, we define the block matrix composed of the orthonormal eigenvectors, $\mathbf{U} = (\mathbf{U}_0, \mathbf{U}_1, \dots, \mathbf{U}_{N-1})$, with $\mathbf{U}_p = (f_{1,p}, f_{2,p}, \dots, f_{N,p})^T$, which diagonalizes the matrix \mathbf{A} as

$$\mathbf{U}^T \mathbf{A} \mathbf{U} = \begin{pmatrix} \lambda_0 & 0 & \cdots & 0 \\ 0 & \lambda_1 & \cdots & 0 \\ \vdots & \vdots & \ddots & \vdots \\ 0 & 0 & \cdots & \lambda_{N-1} \end{pmatrix}. \quad (\text{A.24})$$

The normal coordinates are finally described as

$$\mathbf{X} = \mathbf{U}^T \mathbf{R}, \quad (\text{A.25})$$

with the element

$$\mathbf{X}_p = \sqrt{\frac{1}{N}} \sum_{n=1}^N \mathbf{r}_n(t) \left[\cos\left(\frac{2\pi np}{N}\right) + \sin\left(\frac{2\pi np}{N}\right) \right], \quad (\text{A.26})$$

for the ring polymer chain.

From Eq. (A.4), the normal coordinates of mode p obeys the following equation:

$$\frac{d\mathbf{X}_p}{dt} = -\frac{k}{\zeta} \lambda_p \mathbf{X}_p + \mathbf{W}_p, \quad (\text{A.27})$$

where $\mathbf{W}_p = \mathbf{U}^T \mathbf{W}$ is the random force, which satisfies

$$\langle \mathbf{W}_p(t) \cdot \mathbf{W}_q(t') \rangle = 6k_B T \zeta^{-1} \delta_{p,q} \delta(t - t'). \quad (\text{A.28})$$

The formal solution of Eq. (A.27) is given by

$$\mathbf{X}_p(t) = \mathbf{X}_p(0) \exp(-t/\tau_p) + \int_0^t dt' \mathbf{W}_p(t') \exp(-(t - t')/\tau_p), \quad (\text{A.29})$$

where

$$\tau_p = \frac{\zeta}{k\lambda_p} = \frac{\zeta}{4k \sin^2\left(\frac{\pi p}{N}\right)} \quad (\text{A.30})$$

represents the Rouse relaxation time. The autocorrelation function of $\mathbf{X}_p(t)$ is generally described by

$$\langle \mathbf{X}_p(t) \cdot \mathbf{X}_p(0) \rangle = \frac{3k_B T}{k\lambda_p} \exp(-t/\tau_p). \quad (\text{A.31})$$

The static correlation of the Rouse mode is expressed as

$$\langle \mathbf{X}_p(0)^2 \rangle = \frac{3k_B T}{k\lambda_p} = \frac{b^2}{4 \sin^2\left(\frac{\pi p}{N}\right)} \quad (\text{A.32})$$

from the the initial value of Eq. (A.31).

ACKNOWLEDGMENTS

This work was supported by JSPS KAKENHI Grant Numbers: JP18H01188 (K.K.), JP20H05221 (K.K.), and JP19H04206 (N.M.). This work was also partially supported by the Fugaku Supercomputing Project (No. JPMXP1020200308) and the Elements Strategy Initiative for Catalysts and Batteries (No. JPMXP0112101003) from the Ministry of Education, Culture, Sports, Science, and Technology. The numerical calculations were performed at Research Center of Computational Science, Okazaki Research Facilities, National Institutes of Natural Sciences, Japan.

CONFLICTS OF INTEREST

The authors have no conflicts to disclose.

DATA AVAILABILITY

The data that support the findings of this study are available from the corresponding authors upon reasonable request.

- ¹M. Doi and S. F. Edwards, *The Theory of Polymer Dynamics* (Oxford University Press, Oxford, 1986).
- ²M. E. Cates and J. M. Deutsch, "Conjectures on the statistics of ring polymers," *J. Phys.* **47**, 2121–2128 (1986).
- ³S. P. Obukhov, M. Rubinstein, and T. Duke, "Dynamics of a Ring Polymer in a Gel," *Phys. Rev. Lett.* **73**, 1263–1266 (1994).
- ⁴M. Müller, J. P. Wittmer, and M. E. Cates, "Topological effects in ring polymers: A computer simulation study," *Phys. Rev. E* **53**, 5063–5074 (1996).
- ⁵M. Müller, J. P. Wittmer, and M. E. Cates, "Topological effects in ring polymers. II. Influence of persistence length," *Phys. Rev. E* **61**, 4078–4089 (2000).
- ⁶T. McLeish, "Polymers without beginning or end," *Science* **297**, 2005–2006 (2002).
- ⁷S. Brown and G. Szamel, "Computer simulation study of the structure and dynamics of ring polymers," *J. Chem. Phys.* **109**, 6184–6192 (1998).
- ⁸S. S. Jang, T. Çağın, and W. A. Goddard, III, "Effect of cyclic chain architecture on properties of dilute solutions of polyethylene from molecular dynamics simulations," *J. Chem. Phys.* **119**, 1843–1854 (2003).
- ⁹G. Tsolou, N. Stratikis, C. Baig, P. S. Stephanou, and V. G. Mavrantzas, "Melt Structure and Dynamics of Unentangled Polyethylene Rings: Rouse Theory, Atomistic Molecular Dynamics Simulation, and Comparison with the Linear Analogues," *Macromolecules* **43**, 10692–10713 (2010).
- ¹⁰J. D. Halverson, W. B. Lee, G. S. Grest, A. Y. Grosberg, and K. Kremer, "Molecular dynamics simulation study of nonconcatenated ring polymers in a melt. I. Statics," *J. Chem. Phys.* **134**, 204904 (2011).
- ¹¹J. D. Halverson, W. B. Lee, G. S. Grest, A. Y. Grosberg, and K. Kremer, "Molecular dynamics simulation study of nonconcatenated ring polymers in a melt. II. Dynamics," *J. Chem. Phys.* **134**, 204905 (2011).
- ¹²A. Rosa and R. Everaers, "Ring Polymers in the Melt State: The Physics of Crumpling," *Phys. Rev. Lett.* **112**, 118302 (2014).
- ¹³D. G. Tsalikis, V. G. Mavrantzas, and D. Vlassopoulos, "Analysis of Slow Modes in Ring Polymers: Threading of Rings Controls Long-Time Relaxation," *ACS Macro Lett.* **5**, 755–760 (2016).
- ¹⁴D. G. Tsalikis, T. Koukoulas, V. G. Mavrantzas, R. Pasquino, D. Vlassopoulos, W. Pyckhout-Hintzen, A. Wischniewski, M. Monkenbusch, and D. Richter, "Microscopic Structure, Conformation, and Dynamics of Ring and Linear Poly(ethylene oxide) Melts from Detailed Atomistic Molecular Dynamics Simulations: Dependence on Chain Length and Direct Comparison with Experimental Data," *Macromolecules* **50**, 2565–2584 (2017).
- ¹⁵A. R. Brás, R. Pasquino, T. Koukoulas, G. Tsolou, O. Holderer, A. Radulescu, J. Allgaier, V. G. Mavrantzas, W. Pyckhout-Hintzen, A. Wischniewski, D. Vlassopoulos, and D. Richter, "Structure and dynamics of polymer rings by neutron scattering: breakdown of the Rouse model," *Soft Matter* **7**, 11169 (2011).
- ¹⁶A. R. Brás, S. Gooßen, M. Krutyeva, A. Radulescu, B. Farago, J. Allgaier, W. Pyckhout-Hintzen, A. Wischniewski, and D. Richter, "Compact structure and non-Gaussian dynamics of ring polymer melts," *Soft Matter* **10**, 3649–3655 (2014).
- ¹⁷S. Gooßen, A. R. Brás, M. Krutyeva, M. Sharp, P. Falus, A. Feoktystov, U. Gasser, W. Pyckhout-Hintzen, A. Wischniewski, and D. Richter, "Molecular Scale Dynamics of Large Ring Polymers," *Phys. Rev. Lett.* **113**, 168302 (2014).
- ¹⁸M. Kruteva, M. Monkenbusch, J. Allgaier, O. Holderer, S. Pasini, I. Hoffmann, and D. Richter, "Self-Similar Dynamics of Large Polymer Rings: A Neutron Spin Echo Study," *Phys. Rev. Lett.* **125**, 238004 (2020).
- ¹⁹V. Arrighi and J. S. Higgins, "Local Effects of Ring Topology Observed in Polymer Conformation and Dynamics by Neutron Scattering—A Review," *Polymers* **12**, 1884 (2020).
- ²⁰A. Arbe, F. Alvarez, and J. Colmenero, "Neutron scattering and molecular dynamics simulations: synergetic tools to unravel structure and dynamics in polymers," *Soft Matter* **8**, 8257–8270 (2012).
- ²¹W. Kob, C. Donati, S. J. Plimpton, P. H. Poole, and S. C. Glotzer, "Dynamical Heterogeneities in a Supercooled Lennard-Jones Liquid," *Phys. Rev. Lett.* **79**, 2827–2830 (1997).

- ²²C. Donati, S. C. Glotzer, P. H. Poole, W. Kob, and S. J. Plimpton, "Spatial correlations of mobility and immobility in a glass-forming Lennard-Jones liquid," *Phys. Rev. E* **60**, 3107–3119 (1999).
- ²³E. J. Saltzman and K. S. Schweizer, "Non-Gaussian effects, space-time decoupling, and mobility bifurcation in glassy hard-sphere fluids and suspensions," *Phys. Rev. E* **74**, 061501 (2006).
- ²⁴B. Mei, Z. E. Dell, and K. S. Schweizer, "Microscopic Theory of Long-Time Center-of-Mass Self-Diffusion and Anomalous Transport in Ring Polymer Liquids," *Macromolecules* **53**, 10431–10445 (2020).
- ²⁵K. Kremer and G. S. Grest, "Dynamics of entangled linear polymer melts: A molecular-dynamics simulation," *J. Chem. Phys.* **92**, 5057–5086 (1990).
- ²⁶S. Plimpton, "Fast parallel algorithms for short-range molecular dynamics," *J. Comput. Phys.* **117**, 1–19 (1995).
- ²⁷S. K. Sukumaran, G. S. Grest, K. Kremer, and R. Everaers, "Identifying the primitive path mesh in entangled polymer liquids," *J. Polym. Sci. B Polym. Phys.* **43**, 917–933 (2005).
- ²⁸K. Hagita and T. Murashima, "Effect of chain-penetration on ring shape for mixtures of rings and linear polymers," *Polymer* **218**, 123493 (2021).
- ²⁹A. Kopf, B. Dünweg, and W. Paul, "Dynamics of polymer "isotope" mixtures: Molecular dynamics simulation and Rouse model analysis," *J. Chem. Phys.* **107**, 6945–6955 (1997).
- ³⁰J. M. Wiest, S. R. Burdette, T. W. Liu, and B. R. Bird, "Effect of ring closure on rheological behavior," *J. Non-Newton Fluid* **24**, 279–295 (1987).
- ³¹P. M. Rauscher, K. S. Schweizer, S. J. Rowan, and J. J. de Pablo, "Dynamics of poly[n] catenane melts," *J. Chem. Phys.* **152**, 214901 (2020).
- ³²D. Pan and Z.-Y. Sun, "Diffusion and Relaxation Dynamics of Supercooled Polymer Melts," *Chinese J. Polym. Sci.* **36**, 1187–1194 (2018).
- ³³M. Aichele, Y. Gebremichael, F. W. Starr, J. Baschnagel, and S. C. Glotzer, "Polymer-specific effects of bulk relaxation and stringlike correlated motion in the dynamics of a supercooled polymer melt," *J. Chem. Phys.* **119**, 5290–5304 (2003).
- ³⁴S. Peter, H. Meyer, and J. Baschnagel, "MD simulation of concentrated polymer solutions: Structural relaxation near the glass transition," *Eur. Phys. J. E* **28**, 147–158 (2009).
- ³⁵J.-L. Barrat, J. Baschnagel, and A. Lyulin, "Molecular dynamics simulations of glassy polymers," *Soft Matter* **6**, 3430 (2010).
- ³⁶J. S. Shaffer, "Effects of chain topology on polymer dynamics: Configurational relaxation in polymer melts," *J. Chem. Phys.* **103**, 761–772 (1995).
- ³⁷J. T. Padding and W. J. Briels, "Time and length scales of polymer melts studied by coarse-grained molecular dynamics simulations," *J. Chem. Phys.* **117**, 925–943 (2002).
- ³⁸J. T. Kalathi, S. K. Kumar, M. Rubinstein, and G. S. Grest, "Rouse Mode Analysis of Chain Relaxation in Homopolymer Melts," *Macromolecules* **47**, 6925–6931 (2014).
- ³⁹H.-P. Hsu and K. Kremer, "Detailed analysis of Rouse mode and dynamic scattering function of highly entangled polymer melts in equilibrium," *Eur. Phys. J. Special Topics* **226**, 693–703 (2017).
- ⁴⁰Z. Wang, A. E. Likhtman, and R. G. Larson, "Segmental Dynamics in Entangled Linear Polymer Melts," *Macromolecules* **45**, 3557–3570 (2012).
- ⁴¹M. E. Cates, M. Fuchs, K. Kroy, W. C. K. Poon, and A. M. Puertas, "Theory and simulation of gelation, arrest and yielding in attracting colloids," *J. Phys.: Condens. Matter* **16**, S4861–S4875 (2004).
- ⁴²D. R. Reichman, E. Rabani, and P. L. Geissler, "Comparison of Dynamical Heterogeneity in Hard-Sphere and Attractive Glass Formers," *J. Phys. Chem. B* **109**, 14654–14658 (2005).
- ⁴³E. Flenner and G. Szamel, "Relaxation in a glassy binary mixture: Mode-coupling-like power laws, dynamic heterogeneity, and a new non-Gaussian parameter," *Phys. Rev. E* **72**, 011205 (2005).
- ⁴⁴D. Michieletto, D. Marenduzzo, E. Orlandini, G. P. Alexander, and M. S. Turner, "Threading Dynamics of Ring Polymers in a Gel," *ACS Macro Lett.* **3**, 255–259 (2014).
- ⁴⁵D. Michieletto, D. Marenduzzo, E. Orlandini, G. P. Alexander, and M. S. Turner, "Dynamics of self-threading ring polymers in a gel," *Soft Matter* **10**, 5936–5944 (2014).
- ⁴⁶E. Lee, S. Kim, and Y. Jung, "Slowing Down of Ring Polymer Diffusion Caused by Inter-Ring Threading," *Macromol. Rapid Commun.* **36**, 1115–1121 (2015).
- ⁴⁷D. Michieletto and M. S. Turner, "A topologically driven glass in ring polymers," *Proc. Natl. Acad. Sci. U.S.A.* **113**, 5195–5200 (2016).
- ⁴⁸D. Michieletto, D. Marenduzzo, E. Orlandini, and M. Turner, "Ring Polymers: Threadings, Knot Electrophoresis and Topological Glasses," *Polymers* **9**, 349 (2017).
- ⁴⁹D. Michieletto, N. Nahali, and A. Rosa, "Glassiness and Heterogeneous Dynamics in Dense Solutions of Ring Polymers," *Phys. Rev. Lett.* **119**, 197801 (2017).
- ⁵⁰T. Sakaue, "Topological free volume and quasi-glassy dynamics in the melt of ring polymers," *Soft Matter* **14**, 7507–7515 (2018).
- ⁵¹E. Lee and Y. Jung, "Slow Dynamics of Ring Polymer Melts by Asymmetric Interaction of Threading Configuration: Monte Carlo Study of a Dynamically Constrained Lattice Model," *Polymers* **11**, 516 (2019).
- ⁵²D. Michieletto and T. Sakaue, "Dynamical Entanglement and Cooperative Dynamics in Entangled Solutions of Ring and Linear Polymers," *ACS Macro Lett.* **10**, 129–134 (2021).
- ⁵³M. Ceriotti, M. Parrinello, T. E. Markland, and D. E. Manolopoulos, "Efficient stochastic thermostating of path integral molecular dynamics," *J. Chem. Phys.* **133**, 124104 (2010).